Annual Report 2024
RACEMAT / WP1

Radionuclides' transport in cementitious materials

Juuso Sammaljärvi, Xiaodong Li, Marja Siitari-Kauppi
University of Helsinki[1]

Jukka Kuva, Ester Jolis, Evgeni Kortunov,
Muhammad Muniruzzaman, Mohammad Jooshaki
Geological Survey of Finland[2]

Contents

Abstract

Diffusion properties of the pristine model concrete material from waste hall cavern lining were studied with the through-diffusion experiments using selected radionuclides: HTO, organic C-14, Cl-36 and Ni-63. The samples from Loviisa LILW repository were drilled and the samples were sent to University of Helsinki for sub-sampling. Sub-samples were prepared for different through-diffusion experiments and structural analyses. The through-diffusion experiments with different radio-tracer cocktails started in 2023 were continued, with one set of parallel experiments stopped in 5/2024 for post-mortem examination.. Post-mortem autoradiographic examination is planned to start after the through-diffusion experiments have been stopped. Structural analyses comprising X-ray tomography, µXRF analysis, water gravimetry and C-14-PMMA auto-radiography have been done. X-ray tomography results yielded 3D structural information on the concrete structure. µXRF confirmed that the cement matrix was homogeneous in elemental composition while the rock aggregate had heterogene-ous composition typical of crystalline rock. Some parts of the rock aggregate had iron in them, which could have an effect on redox sensitive elements. Water gravimetry gave bulk porosity values of concrete. The values were in the range of 6-9 %. C-14-PMMA autoradiography gave results on the bulk porosity and also the spatial distribution of porosity. The bulk porosity by autoradiography was in the range of 8- 10 %. The spatial distribution of porosity results showed that most the porosity was concentrated in the cement matrix while the rock aggregates were mostly nonporous. Modelling efforts have progressed from mostly scoping calculations to the determination of diffusion coefficients for HTO and speciation analysis for nickel tracer.

1. Research topic, background and motivation

1.1 Background and state-of-the-art

Low- and Intermediate Level Waste (LILW) from Finnish nuclear power plants (NPPs) operated by Fortum and TVO will be disposed of in geological on-site repositories. LILW to be disposed of includes radioactive waste generated during operation and decommissioning phases. According to the Loviisa LILW Repository Safety Case Main Report (Nummi, 2018), the various radioactive wastes produced at the Loviisa NPP can be divided into operational waste, decommissioning waste and spent nuclear fuel. Spent nuclear fuel is disposed of in Olkiluoto repository but operational and decommissioning wastes are deposited in Loviisa LILW waste repository. The radioactivity originates from neutron activation (either directly or as fission products) in the reactor core and the structures surrounding the core. The operational wastes are classified as liquid wastes or (solid) maintenance waste. The liquid wastes often include ion exchange resins from different filtering where they are used to remove impurities. They can also be boron and salt-containing evaporator condensates from processing drainage waters, or sludge and sediments from drainage waters as a result of precipitation and sedimentation of large particles. All the liquid wastes accumulated are stored at the liquid waste storage. Liquid waste that cannot be cleared from regulatory control needs to be immobilized for safe handling and deposition. The intermediate level wastes are solidified into concrete containers at the solidification plant prior to their disposal in order to produce a stable waste product that limits the radionuclide release. Low level liquid wastes are solidified into concrete in steel drums. In Olkiluoto NPP, wet or intermediate level waste is cast into bitumen but TVO is considering the change to cement as the immobilization medium (Kumpula, et al, 2022).

Besides the LILW material itself, the disposal concept includes various materials in the constructed structures and waste packages. LILW containers are often made of concrete and the waste caverns containing the solidified waste are lined with concrete, forming a concrete basin as in Loviisa, or a silo, as in Olkiluoto. The waste caverns are also planned to be backfilled with concrete upon closure. These engineered barrier systems are surrounded by bedrock, which acts as a natural barrier hindering radionuclide release. It is important to understand the evolution and potential interactions of these materials during the repository timescale. After the repository closure, the structure and evolution of waste material itself may affect the performance of the repository over a long time scale. Concrete structures experience degradation over time due to exposure to surrounding pore waters and the waste material can also degrade over time.

Concretes with different types of compositions are used depending on the specific purpose of the concrete structure. The different purposes might be the forming the concrete basin or silo structure of the waste cavern, acting as a waste container or part of it, as the waste immobilization material or as the cavern backfill material. Different recipes might be needed to build a sound structure lining the waste cavern or to contain for example ion exchange resin waste (Kotatkova, et al, 2017). Superplasticicers are used to improve workability of concrete and they are especially useful when the concrete is planned to be used as a backfill material and achieving even spreading and mixing is difficult due to cramped conditions or other limitations. A topic of considerable research interest is effect of organic compounds, such as superplasticizers, on the mobility of radionuclides (Young, 2012; Isaacs, et al, 2013). This change in mobility would manifest itself by changes in the diffusion coefficients and distribution coefficients of the concrete material. The transport and retention properties of cementitious materials can vary between different compositions and the values forming the basis for calculations should be preferably based on similar compositions as used in the LILW repository setting to minimise uncertainty. Especially any changes in radionuclide mobility due to differing material compositions should be known in order to lessen conservatism in safety case calculations.

The radionuclide inventory of LILW is commonly composed of activation products, such as C-14, Cl-36, Ni-59 and Ni-63 and also uranium wastes. Other activation and fission products may also be present, as well as the actinides and their progeny. Other nuclides however have a lower contribution to dose and release rates and hence their inventory estimates contain more margin with respect to long-term safety criteria. All these different elements have specific chemical interactions with the barrier systems. Bedrock retards significantly the transport of many radionuclides originating from uranium wastes but has little known retarding effect for C-14 and Cl-36, and only slight effect for Ni-59 and Ni-63. For these radionuclides the retardation of transport is mainly based on the engineered barriers, such as concretes.

The transport of the radionuclides present in LILW in cementitious materials has been studied with batch sorption experiments to investigate the sorption processes and with diffusion experiments to study the diffusion behaviour. Batch sorption

experiments have shown that the retention properties of C-14 depend strongly on whether it is in an organic or inorganic form. Inorganic species of C-14 can adsorb to positive sites or precipitate as carbonates but organic C-14-species tend to often only weakly adsorb on surfaces (Evans, 2008). There are however differences between organic compounds, ranging from very weak bonding to a small amount of selective binding for the formate, presumably into ettringite (Wieland, et al, 2016). Differing cement matrices were also shown to have very different diffusion coefficients for C-14-acetate species. Cl-36 sorbs into cement by forming chloride and oxychloride compounds. In some conditions, it can form Friedel's and Kuzel's salts. Sorption, or secondary phase formation, depends on the type of binder and the nature of the cations in the pore solution (Evans, 2008). The retention of Cl-36 by cementitious backfill has been studied by (Van Es, et al., 2015). They found out that the breakthrough of Cl-36 is dependent of chloride concentration and sorption like process takes place. The spatial distribution of the Cl-36 has been in NVRB cement paste (Van Es, et al., 2015) and in CEMV-based concrete (Macé et al, 2019) by storage phosphor screen autoradiography (SPA). Nickel has been found to sorb considerably into cement phases, especially into hydroxides, with coprecipation or surface complexation as a possible mechanism. Nickel species also tend to have low solubility at high pH. This together with sorption leads to immobilisation in cement (Evans, 2008). This feature retards the diffusion of nickel isotopes until the concrete barrier degrades (Nummi, 2018).

Our research group has long been involved in studies of the interactions of cementitious materials with the repository environment especially in co-operation with the French Nuclear Safety Institute (IRSN). The mineralogical and microstructural evolution of Portland cement paste in contact with argillite was studied especially with regard to diffusion and porosity properties (Lalan, et al, 2019). The changes brought by exposure of Low-pH cement to calcareous and argillite pore water were also a focus of another study (Neji, et al, 2022). Our work also contributed to the reactive transport modelling of cement model systems under degradation (Seigneur, et al, 2017). Our research group has also pioneered the use of novel autoradiographic techniques to study the diffusion of radionuclides and porous space where the diffusion takes place. C-14-PMMA autoradiography was originally developed to study the porosity of low porosity crystalline rock (Siitari-Kauppi, 2002) but has since been successfully used to study high porosity materials such as sedimentary rock and cementitious materials (Sammaljärvi, 2017; Lalan, et al, 2019; Neji, et al, 2022). During KYT2022-funded RASK project we developed methods to study and image the transport of radionuclides in concretes and their interfaces with crystalline rock.

1.2 Objectives and expected results of WP1

We study diffusion and retention behaviour of long-term safety-relevant radionuclides in cementitious materials found specifically in the LILW repository. We will focus on the main concrete structures found in the LILW repository: the waste cavern concrete and the backfill concrete that will be found around the waste packages in considerable volume. The results, such as diffusion and distribution coefficients, from this study will then increase the robustness of the safety case calculations for LILW repositories and build confidence. This study will build on the existing know-how and experience in our research group concerning structural characterisation and diffusion study methods. These methods can be applied in the scope of this work and would constitute a validation of those techniques for LILW repository-relevant concrete types and safety case-important radionuclides. Ni-63 post mortem autoradiography will be one of the focus of this work because it has not been studied earlier extensively with autoradiography in the context of cementitious materials in a repository environment.

The experiments performed in the scope of this research project will produce several concrete results. The diffusion experiments will produce apparent and effective diffusion coefficients, and distribution coefficients for HTO, Cl-36 and Ni-63 in realistic concrete material environments. Post-mortem examinations will also provide information on the spatial distribution of retention, highlighting possible heterogeneities in the retention behaviour of radionuclides. The structural characterisation will provide realistic information on the structure of in situ materials. The coefficients produced for Ni-63 are also valid for another important isotope, Ni-59, as the isotopes have similar chemistry. This brings more certainty to estimating the retarding effect of the concrete on the diffusion of these radionuclides. The results can be applied in the LILW repository safety case calculations. While this study focuses on the behaviour of radionuclides in pristine materials, the results can be used as a basis for studying the evolution of concrete structures, considering the combined impact of various processes) contributing to the concrete degradation over time scale of repository use. Overall the results from this research project will promote the safe use of nuclear energy by decreasing uncertainties associated with LILW disposal.

2. Work package 1, Diffusion experiments

2.1 Overall work plan

Diffusion properties of the pristine model concrete material from waste hall cavern lining and later on from different backfill concrete recipes, was studied with the through-diffusion experiments using selected radionuclides: HTO, organic C-14, Cl-36 and Ni-63 (T1.1). The work started with the acquisition of samples from end-user organizations. The samples are envisioned to be model matrix samples without radioactivity. The expected outcome of this experiment is the effective diffusion coefficients and partition coefficients for the specified radionuclides by fitting experimental results and diffusion modelling together with the aid of COMSOL and PhreeqC modelling. In addition, the development of modelling tools for taking into account the heterogeneous composition of the material will be started on the 3D cement model matrices.

After the diffusion experiment, the experimental setups will be dismantled and post-mortem autoradiography will be performed to ascertain the spatial distributions of radioactivity (T1.2). Supporting porosity analyses by C-14-PMMA autoradiography and water gravimetry was done to obtain bulk porosity values and spatial distributions of porosity. The C-14-PMMA porosity results will be combined with structural information from XCT and µXRF (T1.3). The results from through-diffusion experiments and post-mortem autoradiography analyses will be modelled in order to obtain values for diffusion coefficients and distribution coefficients.

2.2 Sample preparation

The samples from the Loviisa LILW repository were drilled and the sample core (Figure 1) were sent to the University of Helsinki for sub-sampling. Two parallel drill cores (Sample codes LO106 and LO110) were received.

Figure 1 Photo of the LILW repository basin concrete sample core LO110.

The work on the drill cores began with sample preparation. The sample material was then worked sawed into suitable cylinder-shaped sub-samples which as shown in Figure 2, presenting the sawing scheme used.

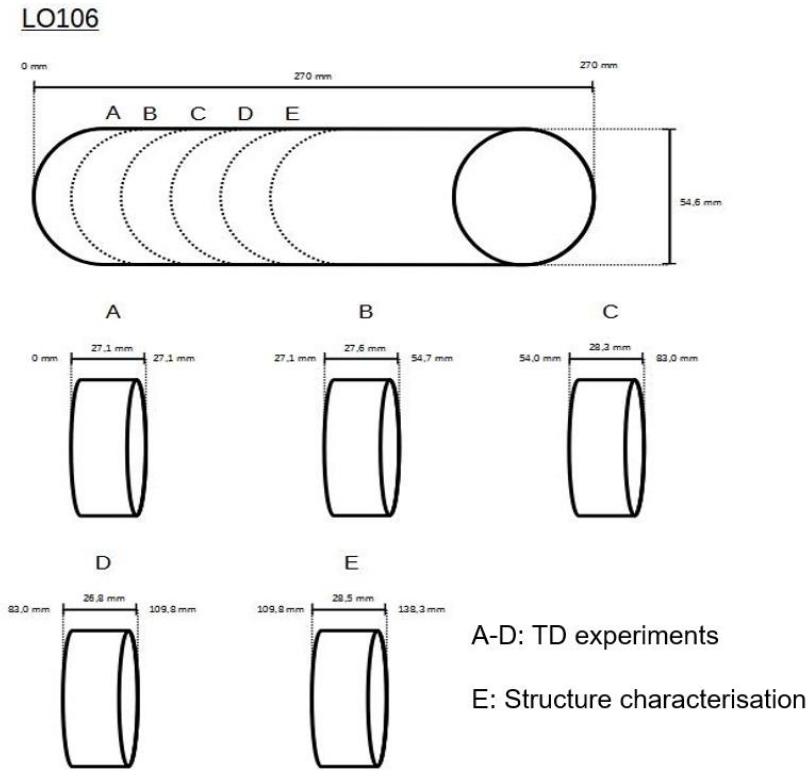

Figure 2 Sawing scheme for sample LO106.

Sub-samples were prepared for different through-diffusion experiments (Sub-samples A-D) and structural analyses (Sub-samples E) with a length of roughly 3 cm and diameter of 5.5 cm and structural analyses. For the diffusion experiments the sub-samples were set into through-diffusion chambers and thereafter the chambers and the samples were equilibrated in cement pore water simulant. One set of through-diffusion samples (Sub-samples A) was kept in reserve. The cement material composition information (Table 1) was obtained from Fortum.

Table 1 LILW repository basin concrete composition

Component	Amount (kg/m3)
CEMIII	130
Blast furnace slag	230
Silica	12
Water	152
Water/Cement Ratio	0.35

2.3 Experimental Methods and Results

2.3.1 Task 1 (T1.1), Through-diffusion experiments

2.3.1.1 Summary of 2023

The work in T1.1 began with sample preparation. The sample material was then worked into suitable cylinder-shaped sub-samples which were set into through-diffusion chambers. Before the diffusion experiments were started, the chambers and the samples were equilibrated in cement pore water simulant.

Through-diffusion experiments were started with selected radionuclides: HTO, organic C-14, Cl-36 and Ni-63. The experiments are started by spiking the inlet solutions with radionuclide solutions. Following tracer cocktails were prepared as shown in Table 2.

Table 2 Summary of tracer cocktails in the through diffusion experiments started May 2023.

Tracer Cocktail	Samples	Inert Tracer Activity HTO (Bq/ml)	Reactive Tracer Activity (Bq/ml)
HTO+formate C-14	LO106B & LO110B	5000	2000 (formate C-14)
HTO+Cl-36	LO106C & LO110C	5000	500 (Cl-36)
HTO+Ni-63	LO106D & LO110D	5000	500 (Ni-63)

HTO+C-14, HTO+Cl-36 and HTO+Ni-63. HTO is present in all the tracer cocktails as it functions as a conservative tracer that gives therefore pure effective diffusion coefficient values, while the other tracers are known to experience at least some amount of retention in cementitious materials. Activities were thereafter followed weekly in both inlet- and outlet chambers by Liquid Scintillation Counting. The expected outcome of this experiment together with modelling will be the effective diffusion coefficients and partition coefficients for the specified radionuclides.

The liquid volume that was collected from the outlet chambers for sampling was replaced by a similar volume of fresh synthetic pore water simulant to maintain zero concentration border condition and a concentration gradient across the sample setup. The liquid scintillation counting was done with PerkinElmer Tri-Carb 2910-TR liquid scintillation counter. The samples were prepared by mixing 5 ml of sample solution and 15 ml of UltimaGold (PerkinElmer) liquid scintillation cocktail. Liquid scintillation background measurements were performed in a similar way using synthetic cement pore water without radiotracers. The counting efficiencies for the tracers were determined by measuring a solution with a known tracer activity in different quenched solutions (a mixture with variable water: acetone ratio as a quencher). The measurement time was 30 minutes per sample.

The activities measured from the inlet chambers were plotted as a decrease of activity over time while the outlet chamber data was plotted as cumulative activity increases over time. All the experiments were conducted in a nitrogen glovebox, with the oxygen concentrations staying mostly under 10 ppm and the carbon dioxide concentration mostly less than 1 ppm. This precludes cement carbonation-related degradation during the experiment and mimics the anoxic post-closure repository conditions.

2.3.1.2 Work in 2024

In 2024 we continued the diffusion experiments started in 2023. One set of parallel samples (LO106B, LO106C and LO106D) where terminated at the end of 5/2024 (12 months) to start the post-mortem examination. Another set (LO110B, LO110C and LO110D) are planned to be continued until the end of 2024 (18 months).

Results for HTO+C-14 through-diffusion experiments are shown in Figure 3. It can be seen that there is about 84 % of HTO left in the Inlet chambers. 99 % of C-14- formic acid is also still in the Inlet chambers. About 0.05- 0.33 % HTO cumulative activity is found in the Outlet chambers. No C-14 activity in outlet has been detected in the Outlet chambers.

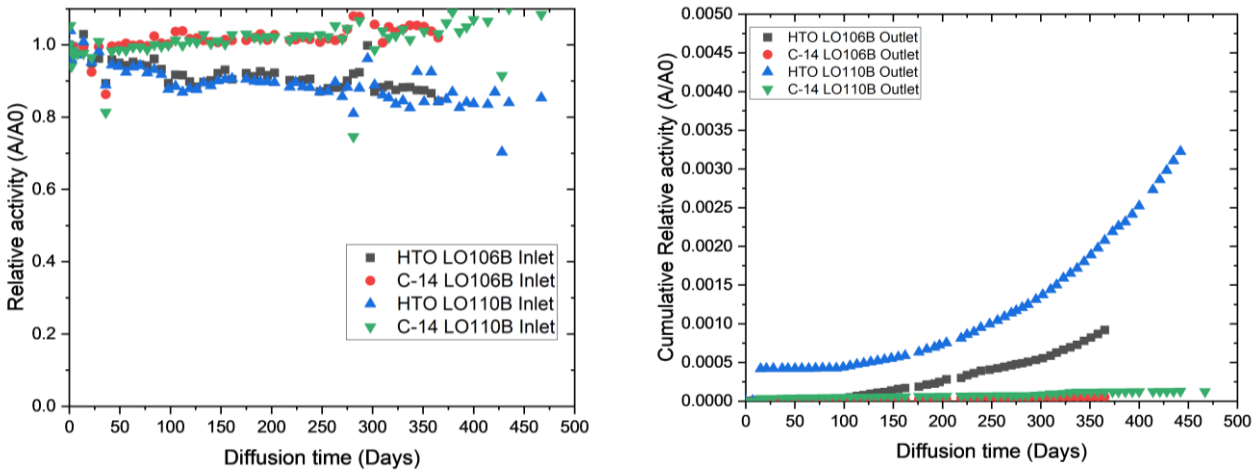

Figure 3 HTO+C-14- through-diffusion results. Left: Inlet chamber relative activities. Right: Outlet chamber relative activities.

Results for HTO+Cl-36 through-diffusion experiments are shown in Figure 4. It can be seen that there is about 85 % of HTO left in the Inlet chambers. 99 % of Cl-36 is also still in the Inlet chambers. About 0.05- 0.33 % HTO cumulative activity is found in the Outlet chambers. No Cl-36 activity in outlet has been detected in the Outlet chambers.

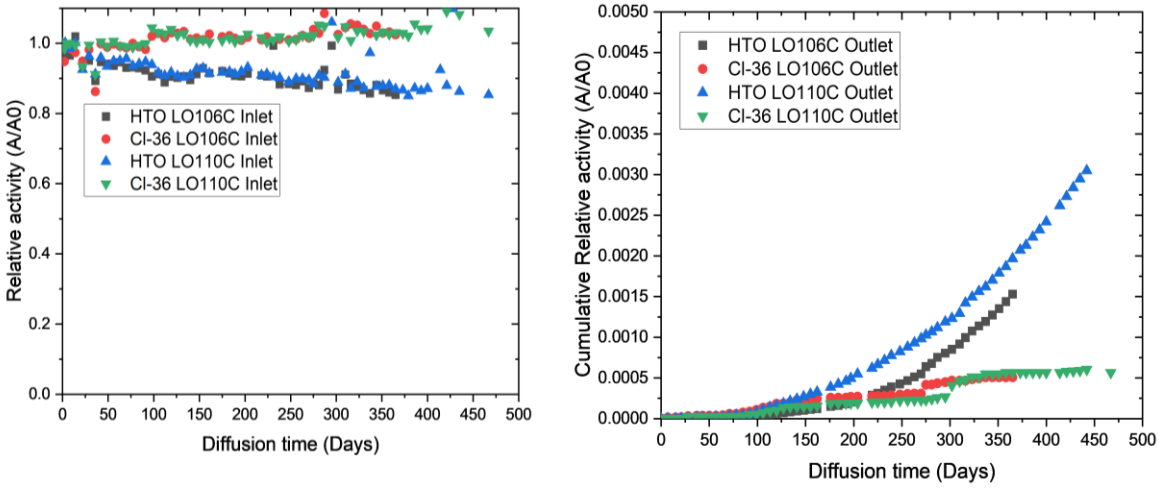

Figure 4 HTO+Cl-36- through-diffusion results. Left: Inlet chamber relative activities. Right: Outlet chamber relative activities.

Results for HTO+Cl-36 through-diffusion experiments are shown in Figure 5Figure 4. It can be seen that there is about 87 % of HTO left in the Inlet chambers. 90 % of Cl-36 is also still in the Inlet chambers. About 0.12- 0.18 % HTO cumulative activity is found in the Outlet chambers. No Ni-63 activity in outlet has been detected in the Outlet chambers, besides possible artefacts or contamination. Ni-63 was noted to have an initial decrease of relative activity in the Inlet chambers, followed by gradual increase. Possible reason for Ni-63 behaviour could be precipitation, followed by slow dissolution to solution.

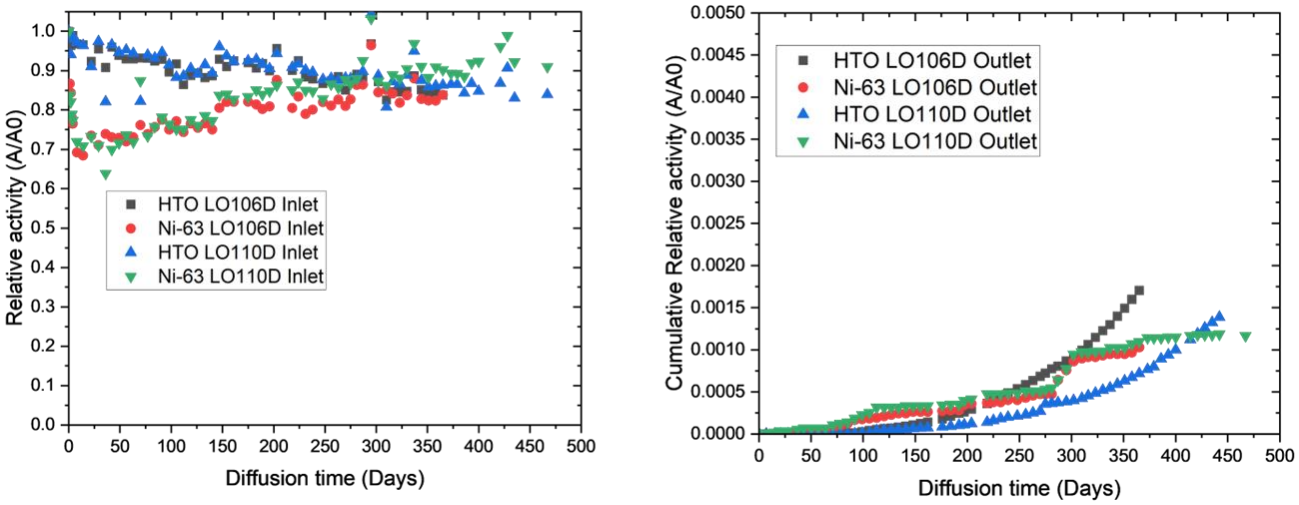

Figure 5 HTO+Ni-63- through-diffusion results. Left: Inlet chamber relative activities. Right: Outlet chamber relative activities.

HTO effective diffusion coefficients were estimated to be around 4-8x10^{-13} m^2/s based on scoping calculations performed in 2023. As more data was gathered during 2024, more reliable modelling could be performed as part of T.1.4.

2.3.2 Task 2 (T1.2), Post-mortem autoradiography

After the diffusion experiments are completed, they will be dismantled. This task will be started in late 2023 or early 2024. Following dismantling the concrete samples will be cut along the diffusion axis and the spatial distributions of activity and locations of the diffusion front are to be ascertained. The result shows the diffusion profile of the studied radioactive element. Quantitative autoradiography requires activity standards, which will produced as part of this work.

Spatial distributions of sorbed tracer activities on the concrete samples are to be measured by storage phosphor screen autoradiography with imaging plates (SPA) scanned with a Fuji FLA-5100 scanner, and the micro-pattern gas detector-based autoradiography (MPGDA) performed with the BeaQuant imaging system (Donnard, et al, 2009). Both of these autoradiography techniques have complementary strengths and weaknesses (Delayre, et al, 2020). SPA has good sensitivity and a wide linear range and it is quite tolerant of artefacts caused by imperfections in the samples. SPA however doesn't allow nuclide- or radiation-specific imaging. The exposure times needed with SPA are also usually found via trial and error, and in any case, after about 1 week the signal fade will start to affect the results (L'Annuziata, 2003). MPGDA has even better sensitivity and a wide linear range. MPGDA also allows for radiation-type, and in some cases, nuclide-specific imaging based on different radiation energies (Delayre, et al, 2020). The measurement is performed straight from the sample and it detects in real-time pulses coming from the radioactive elements in the sample. There are no imaging plates or films that could be overexposed, allowing the measurement can be continued as long as necessary. The high sensitivity of MPGDA is however a disadvantage in some cases. The technique is sensitive to artefacts resulting from imperfect sample preparations and discontinuities, such as cavities (Billon, et al, 2019). Therefore, it is sensible to use two techniques of autoradiography to obtain a comprehensive characterization of the spatial distributions of activity.

In both cases, the specific activities of the studied samples are obtained with the help of standard series containing known amounts of the studied tracer nuclides. The standards are prepared by mixing a known amount of tracer-containing water

solution in a HEMA-MMA-monomer mixture. The resulting mixtures are then polymerized with the aid of AIBN and heated with a graduated heating program developed with Labworldsoft 3.0, with temperatures ranging from 75 to 55 ◦C as described in Sammaljärvi, et al, 2016 (Sammaljärvi, et al, 2016).

Subsequently, thin discs are sawed off from the produced P(HEMA-MMA) copolymer and these discs are then polished, and the polished surfaces are coated with 10 µm of carbon to ensure good electrical conductivity across the disc. Specific activities of standard discs can be used in different autoradiographic techniques for calibrating grey levels for SPA, or cps/mm2 for MPGDA. In SPA autoradiography, they provide a comparison between 16-bit grey scale values and specific activity, while in MPGDA they provide a comparison between cps/mm2 and specific activity.

2.3.2.1 Work in 2024

Post-mortem autoradiography was done on through-diffusion experiments that were stopped in 5/2024. Post-mortem autoradiography was expected to show where the sorbing tracers, C-14, Cl-36 and Ni-63 might have sorbed. The post-mortem autoradiography for the Inlet chamber surface of C-14 through-diffusion cell is shown in Figure 6. This result shows that there is sorption of the C-14-formic acid tracer into the cement matrix of the concrete samples, while the rock aggregate appears more inert towards the tracer.

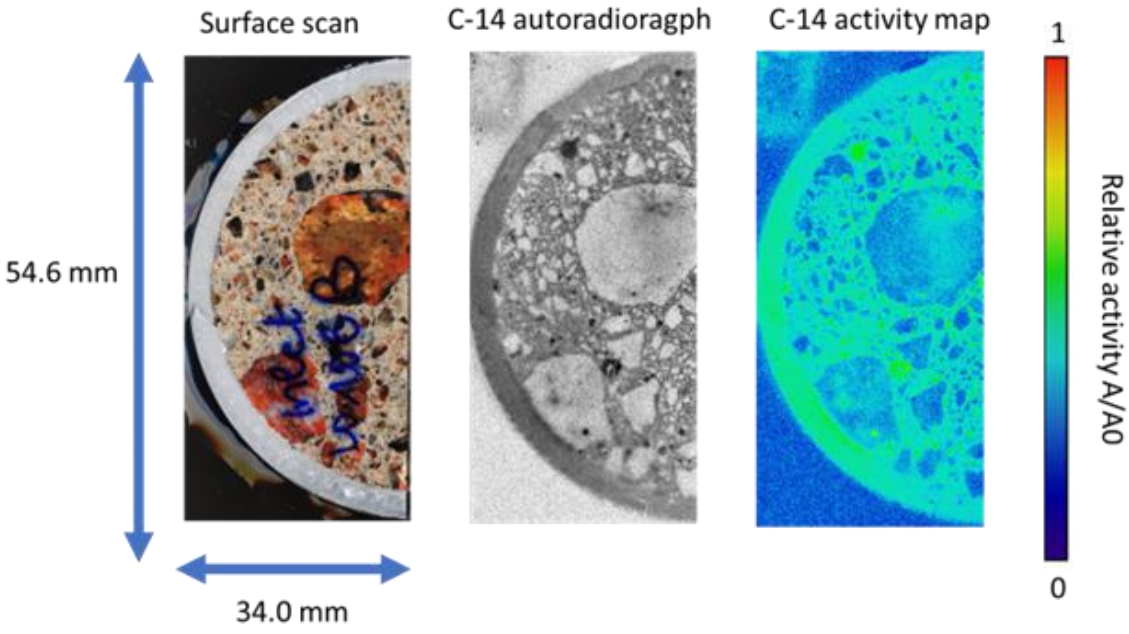

Figure 6 Surface scan (Left), C-14-autoradiograph (Centre) and corresponding C-14 activity map (Right) of the Inlet surface of an HTO+C-14- through-diffusion sample.

Autoradiography results of the cross-section of the HTO+C-14 through-diffusion sample are shown in Figure 7. Based on these results it was determined that the diffusion front had advanced about 5 mm into the sample in 1 year. The sorption into the cement matrix is also visible in the cross-section autoradiography. Overall, the sorption appears to be quite weak and a long exposure time (5 days) was needed to visualise the spatial distribution of activity.

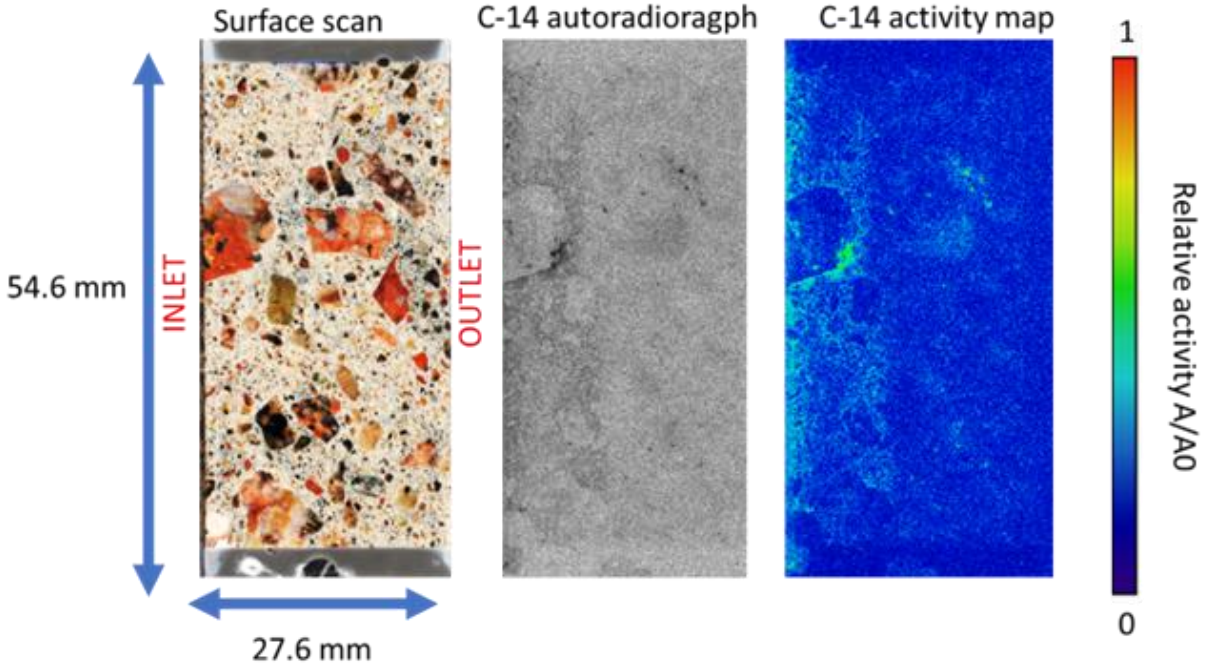

Figure 7 Surface scan (Left), C-14-autoradiograph (Centre) and corresponding C-14 activity map (Right) of the cross-section of a HTO+C-14- through-diffusion sample.

The post-mortem autoradiography for an HTO+Cl-36 through-diffusion sample is shown in Figure 8 .The appears to be clear sorption of Cl-36 tracer into the cement matrix, while the rock aggregate is inert towards the tracer. The autoradiograph appears slightly blurrier than the C-14 autoradiography due to the longer range of the Cl-36 beta emission.

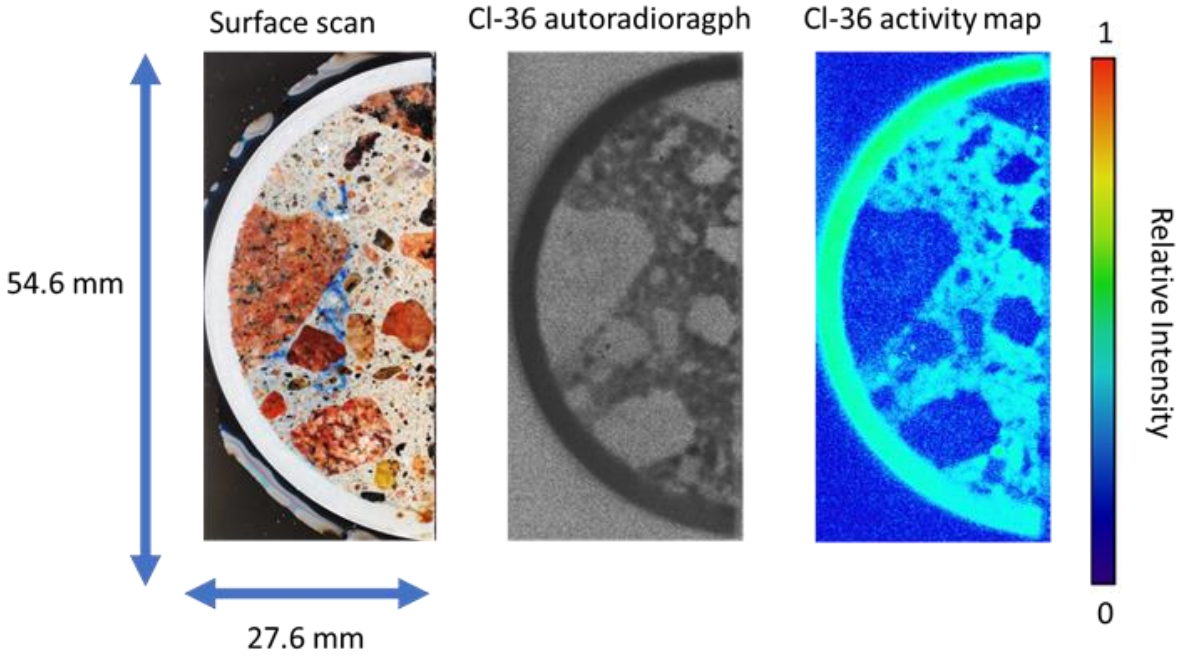

Figure 8 Surface scan (Left),Cl-36-autoradiograph (Centre) and corresponding Cl-36 activity map (Right) of the Inlet surface of a HTO+Cl-36- through-diffusion sample.

Autoradiography results of the cross-section of the HTO+Cl-36 through-diffusion sample are shown in **Error! Reference source not found.**Figure 9Figure 7. Based on this results it was determined that the diffusion front had advanced about 8 mm into the sample in 1 year. The sorption into the cement matrix is also visible in the cross-section autoradiography. The sorption of Cl-36 appears to be considerably stronger than the sorption of C-14 formic acid. Shorter exposure time (2 days) was enough to visualise the spatial distribution of activity.

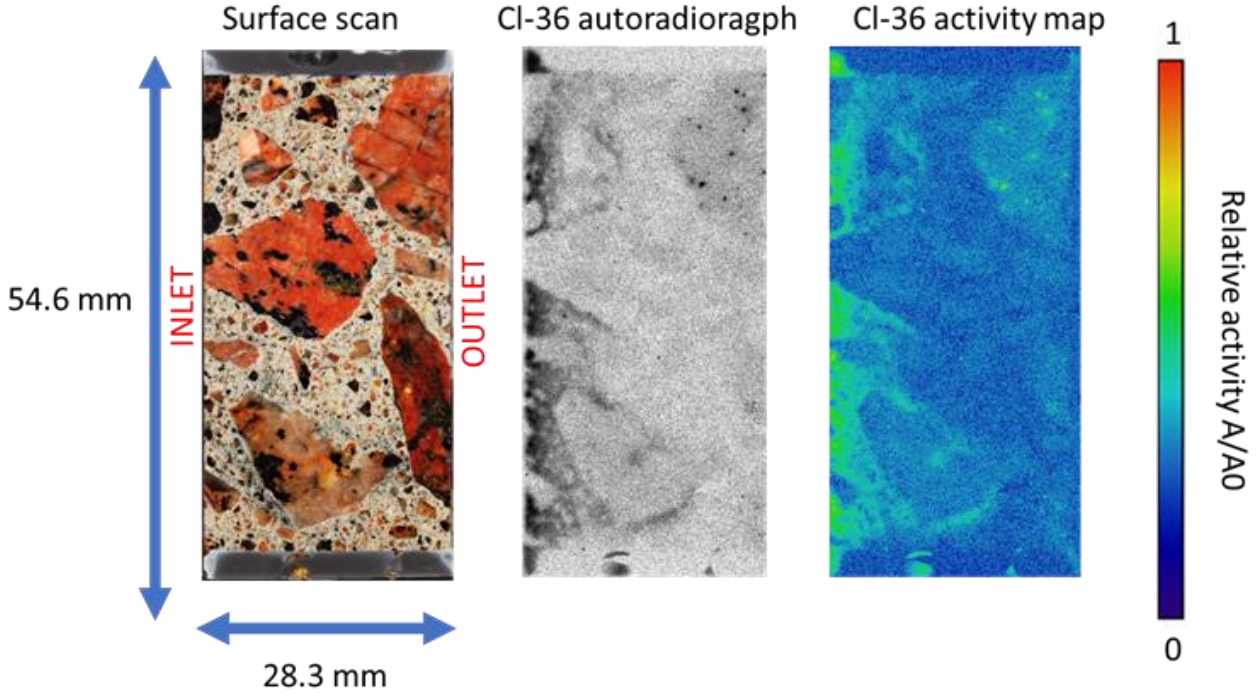

Figure 9 Surface scan (Left), Cl-36 -autoradiograph (Centre) and corresponding Cl-36 activity map (Right) of the cross-section of a HTO+Cl-36 through-diffusion sample.

The post-mortem autoradiography of HTO+Ni-63 through-diffusion is still ongoing. Preliminary autoradiography indicates that diffusion distance has been negligible, leading to subsequent difficulty in visualising sorption. Sorption might also be small due NI being at pH 13 as a neutral hydroxide species. Longer exposure times might be needed for imaging, possibly with the film autoradiography technique.

2.3.3 Task 3 (T1.3), Structure characterisation

Supporting porosity analyses of parallel model matrix samples by C-14-PMMA autoradiography and water gravimetry will be done to obtain bulk porosity values and spatial distributions of porosity. The resulting porosity values can be used in the modelling work as input values. Some analyses will be performed with XCT to obtain 3D structure and µ-XRF will be used to provide mineralogical information. A combination of these techniques has been shown to be a powerful tool. XCT provides 3D structure and density information and C-14-PMMA autoradiography provides highly detailed porosity information (Mazurier, et al, 2016). µ-XRF will be used to obtain chemical mapping on a larger hand specimen scale. This combination of techniques provides a comprehensive data set on the material structure and composition, which can be used to interpret the through-diffusion experiment results. A novel deep learning method will be used to more effectively combine the different methods to obtain 3D mineral and porosity maps.

In water gravimetry, the samples were first dried to a constant weight in a vacuum oven at 55 degrees Celsius. The water gravimetry method used was based on that found in Möri, et al, 2003. After the drying, the samples were immersed in MilliQ water and weighed once a week until a constant weight was achieved, in about three weeks. During the immersion time, the samples were kept in the nitrogen glove box and only removed for weighing. After the water gravimetry measurements, the samples were dried again to constant weight.

For C-14-PMMA autoradiography the samples were immersed in a solution composed of C-14-MMA with an activity concentration of 157.25 kBq/ml and 0.25 (w/w)-% of a thermal initiator, azobisisobutyronitrile (AIBN) and left to immerse for one month. The C-14 stock solution was purchased from Pharmaron UK Ltd, Cardiff, UK. The C-14 was in the form of C-14-labelled methyl methacrylate with a stock solution specific activity of 169 MBq/g. After the immersion period, the samples were polymerised by heating the samples in a heat bath at 55 °C for 16 hours. The polymerised samples were then sawn, cut and polished for autoradiography. The grit used for polishing was Buehler 400(P600) aluminium oxide powder and the polishing liquid was paraffin oil. The autoradiography was done by placing the polished samples on a Fujifilm BAS TR2025 phosphor imaging plate. The exposure time was three days. The imaging plates were scanned, producing digital 16-bit autoradiographs using a Fujifilm FLA-5100 scanner. These autoradiographs were handled digitally and porosity values were calculated with the help of a C-14-activity standard series. In C-14-PMMA autoradiography the grey values of the autoradiographic image are compared with the grey values produced by different specific activity standards. By taking into account the dilution of the C-14 tracer in the sample matrix and the differing densities of the tracer resin and sample matrix, local porosity values can be calculated pixel by pixel. Applying this calculation over the whole area of the sample produces histograms whose mean value represents the mean porosity of the studied area. The C-14-PMMA autoradiography was performed using the Storage Phosphor Autoradiography technique. (Delayre, et al, 2020; Sammaljärvi, et al, 2016; Sardini, et al, 2014).

The XCT analyses were with the GTK XCT scanner: GE Phoenix with accelerating voltage: 10-240 kV (microfocus tube) / 10-180 kV (nanofocus tube), Maximum power: 320 W (microfocus tube) / 20 W (nanofocus tube). The best resolution is given as: 5 µm (microfocus tube) / 900 nm (nanofocus tube), although resolution is usually roughly the sample diameter / 2000 with both tubes (2024 detector pixel columns). Detector is 400x400 mm2 4 MPix temperature stabilized DXR, 200 µm pixel size. The maximum sample size is: 400 mm diameter, 420 mm height, 10 kg weight. The software used for controlling the equipment is FEI PerGeos 2020.2. The samples were mapped by taking about 2500 scans.

The µXRF analyses were obtained with a micro X-ray fluorescence (micro-XRF) Tornado plus (with AMICS) instrument from Bruker at the Geological Survey of Finland (GTK). The system has an Rh X-ray 30-Watt Rh anode target, two simultaneously operating 30mm2 XFlash® silicon drift detectors (SDD) with an energy resolution of < 145 eV at 275 kcps (measured on MnKα) via beryllium windows and poly-capillary optics. Scanning and sample navigation is carried out via a motorized stage which moves the sample beneath the static X-ray beam. No sample preparation was needed. All data acquisition was performed with an accelerating voltage of 50 kV, a beam current of 600 µA using a fixed spot size of 20 µm under 2 mbar vacuum. The samples were mapped in one single run using a step size of 75 µm and a pixel dwell time of 10 ms/pixel.

2.3.3.1 Summary of 2023

Water gravimetric analyses gave bulk porosity values between 6-9 %. most of the porosity was found to be quickly accessible to water. After the first days, there is only a minor porosity value increase and the values plateau. Based on these results, it is likely that 2-4 weeks of impregnation time for C-14-PMMA autoradiography will be enough to fill all of the connected pore networks. The porosity results from C-14-PMMA autoradiography and XCT results are shown in Figure 10. These results show that most of the porosity is concentrated in the cementitious matrix. C-14-PMMA autoradiography yielded total porosity values between 8-10 %. Most of the rock aggregate appears to be low porous, although some aggregates have porosity in them. There are also some bubble-like cavities present where the “porosity” is 100% in the porosity map. Overall, the spatial distribution of porosity is heterogeneous due to the presence of several phases with very different porosities. The total porosity value obtained is a composite value of these different phases. The total porosity values were in the range of 8-10 %. Slight variations in the obtained values can be the result of the fact that autoradiography is a 2D technique, so the porosity value reflects the microstructure of the imaging plane, which might be slightly different from the total value of the whole 3D structure. Overall, the porosity values are however quite close to the bulk porosity values from water gravimetry.

The XCT analysis provides for a full 3D structure of the sample where the major phases (cement, rock aggregate and cavities) are clearly distinguished. Based on this result, it was decided that the through-diffusion samples need to be about 3 cm thick, so that no single rock grain can cut through the sample and therefore provide a potential preferential pathway for radionuclide migration. XCT analyses gave bulk porosity values between 0-3 %. The values are lower than those obtained from water gravimetry and C-14-PMMA autoradiography, as the sample size was too big to provide suitably small

resolution to image the nanoscale porosity in cement, which forms the bulk of the cement porosity. Therefore it can be considered that the portion of porosity seen by XCT with these settings represents the macroporosity.

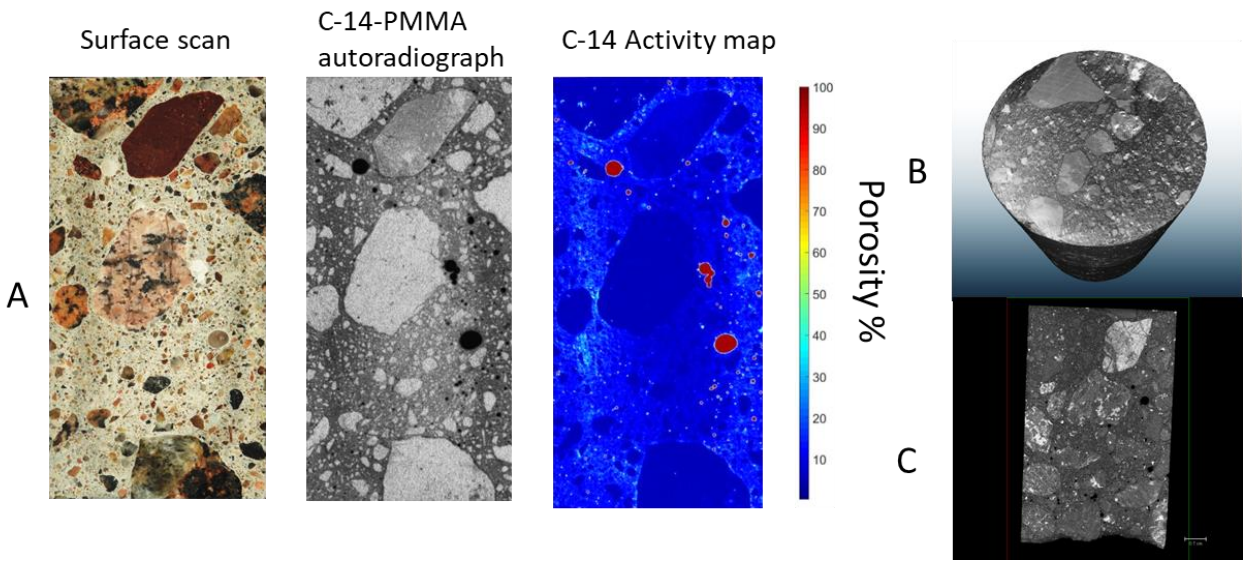

Figure 10 A: C-14-PMMA autoradiography results for LILW basin concrete. Examples of XCT analysis of LILW repository basin concrete sample from drill core LO110. B: Top-Down View. C: Side View.

Summary of the bulk porosity values by different techniques is shown in Table 3.

Table 3 Summary of the bulk porosity values for concrete samples from drill cores LO106 and LO110 by different measurement techniques.

Technique	**Porosity (%)**
Water Gravimetry	6-9
C-14-PMMA Autoradiography	8-10
X-ray Tomography (XCT)	0-3

µXRF analyses were performed to investigate the elemental composition of the cement matrix and the rock aggregate of the concrete samples. µXRF analysis of the cement matrix is presented in Figure 11. According to the elemental analysis, the cement matrix has quite homogeneous distribution of major elements, such as Mg, S and Ca. Elemental analysis shows that the rock aggregate is heterogeneous, crystalline rock. Some rock aggregates have iron in them, raising the possibility that they could possibly have interactions with redox-sensitive tracers.

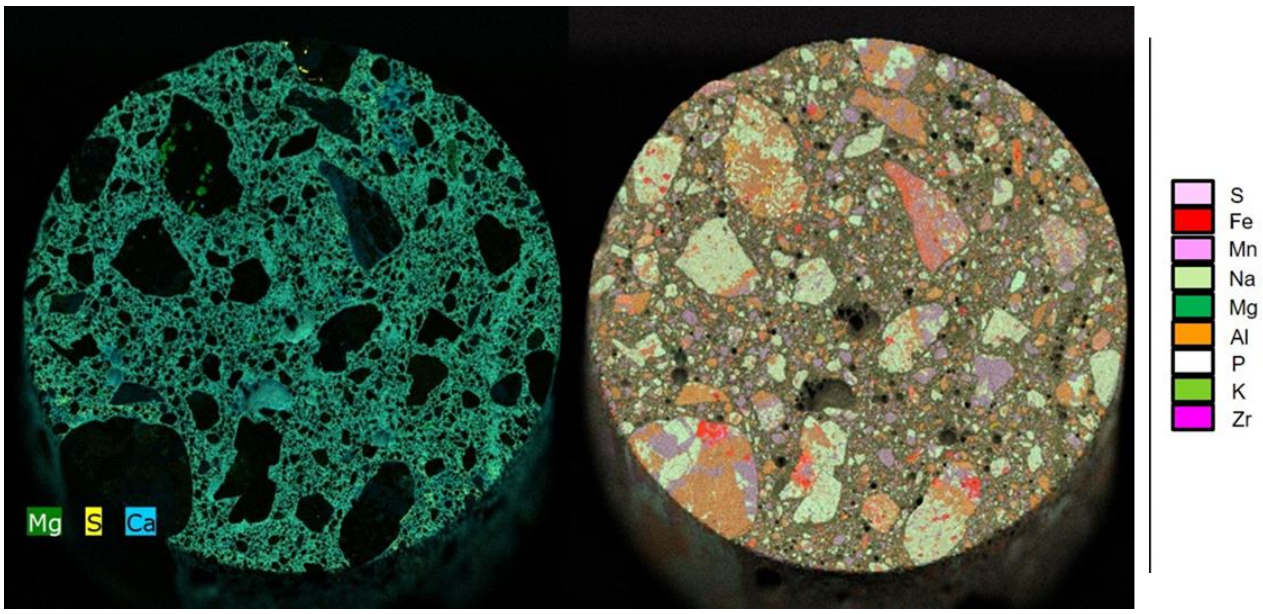

Figure 11 Elemental composition analyses of the cement matrix (left) and rock aggregate (Right) of the LILW repository basin concrete.

2.3.3.2 Work during 2024

During 2024 the structural characterisation performed in 2023 was used in other Tasks of WP1. The porosity values were used as inputs for the modelling in T.1.4. Additional XCT measurements were also performed on the through-diffusion samples LO106B, LO106C and LO106D following the termination of the through-diffusion experiments. Examples of the XCT measurements are shown in Figure 12. These results confirm the finding that there are no cross-cutting fissures or rock aggregates that could affect the diffusion experiments. These results can also be used to support the construction of models incorporating heterogeneous structures.

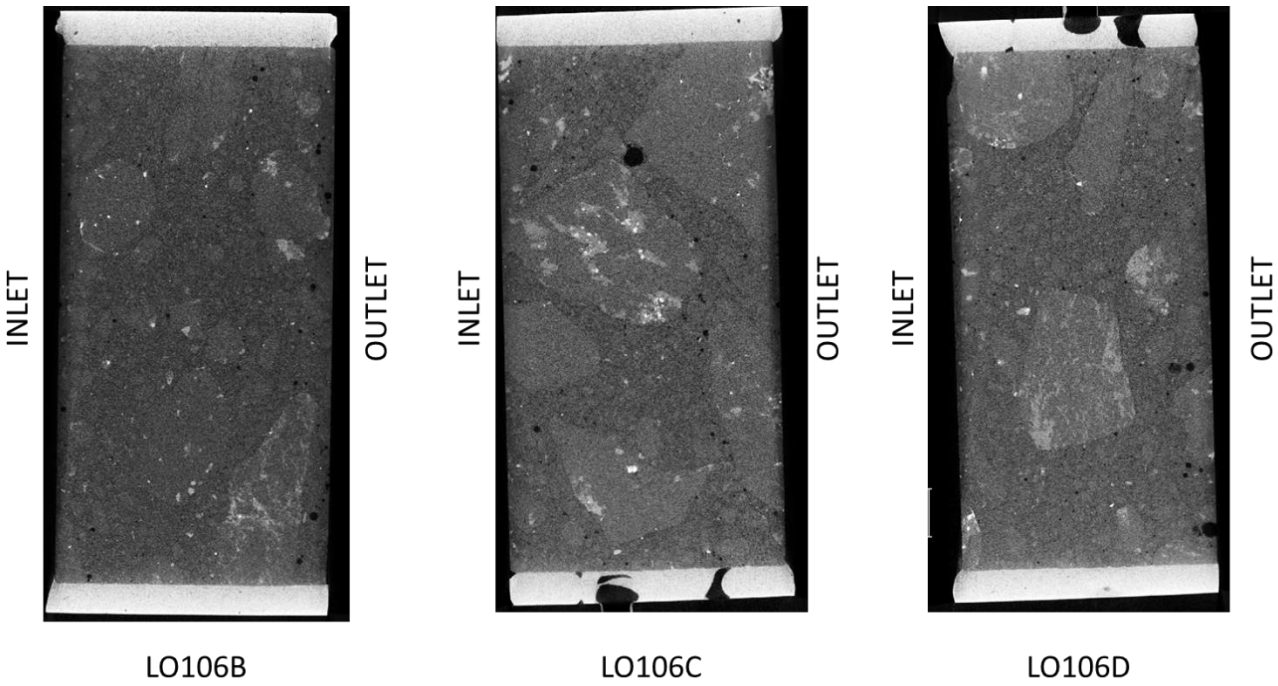

Figure 12 Examples of the XCT measurements for through-diffusion samples LO106B, L=106C and LO106D.

2.3.4 Task 4 (T1.4), Diffusion experiment modelling

The results from through-diffusion experiments are modelled in order to obtain values for diffusion coefficients and distribution coefficients for the studied radionuclides in the 3D concrete matrices. The 3D matrices will be created by coupling techniques of C-14-PMMA autoradiography, XCT and µ-XRF which will provide geometries and properties of realistic matrices of the studied samples. A Time Domain Random Walk (TDRW) model will be developed based on the 3D matrices by considering the pore structure and mineralogical heterogeneity of the concrete samples. Thus, the model to be developed will yield accurate and realistic results of diffusion coefficients and distribution coefficients.

Based on the developed pore scale model, a continuum-scale (or “diffusion-cell-scale”) mechanistic model will be developed by considering a multi-continua approach. The model will explicitly resolve multispecies transport in free water and electrical double layer (EDL) compartments of the pore water, and the diffusive fluxes in these individual compartments will be based on the Nernst-Planck equation. The electrostatic effects in the EDL will be described by the Donnan approximation, whereas the surface exchange/solid solution of cations and anions will be considered. Furthermore, relevant mineral dissolution/precipitation reactions as well as aqueous speciation of chemical species will be explicitly resolved based on the recent thermodynamic databases and by coupling the transport code with PHREEQC. The results of the modelling will allow better parametrization of the diffusion and sorption parameters (e.g. thermodynamic parameters for Ni^{2+} sorption/solid solution and electrostatic sorption behaviour of organic C-14) with the opportunity to cross-validate the results with a range of modelling approaches.

2.3.4.1 Summary of 2023

In 2023 the modelling setup was made based on the structural information obtained in T1.3. While no notable amount of tracers had accumulated in the outlet chambers, scoping calculations were performed to estimate possible breakthrough curves based on diffusion coefficient data from previous experiments. Based on the scoping calculations, it is probable that effective diffusion coefficient for HTO is about 8-4x10^{-13} m^2/s.

2.3.4.2 Work done in 2024

During 2024 the results from through-diffusion experiments were modelled with COMSOL. Ni-63 speciation was also modelled using PHREEQC. This is shown in Figure 13 It can be seen here that the dominant species at the prevalent pH conditions is nickel hydroxide. This species is known to have rather low solubility and therefore saturation index analysis was also performed by PHREEQC. This analysis indicated the species appears to be near the saturation point in this these conditions. Therefore it is possible that minute changes in the solution environment might result in at least partial precipitation. This could be explain the behaviour of the Ni-63 in the through-diffusion experiments.

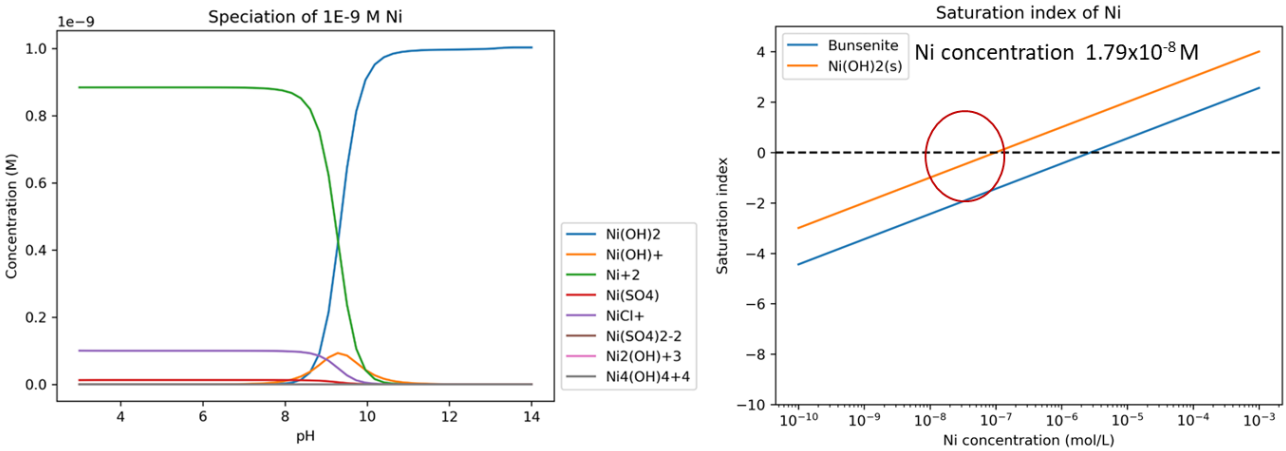

Figure 13 Left: Speciation modelling of Ni by PHREEQC. Right: Saturation index analysis by PHREEQC.

Examples of Through-diffusion modelling curves and experimental data are shown in Figure 14. From these results it can be seen that the D_e for HTO appears to be around 1.8-2.2x10^{-13} m^2/s. This value is fairly low but in the range for concretes based on mixed cements , e.g. Macé, et al, 2019. The values appear to be lower than expected during the year 2023, where the initial estimate for HTO D_e was 4-8x10^{-13} m^2/s. In samples LO106B and LO110C there is part of the curve around 100-300 days that fits less well than the beginning or the end parts of the curves. This could be due to changes in sampling or faster diffusion through some micro-fissure system. One set of diffusion experiments is still ongoing until the end 2024, which will still provide more data points.

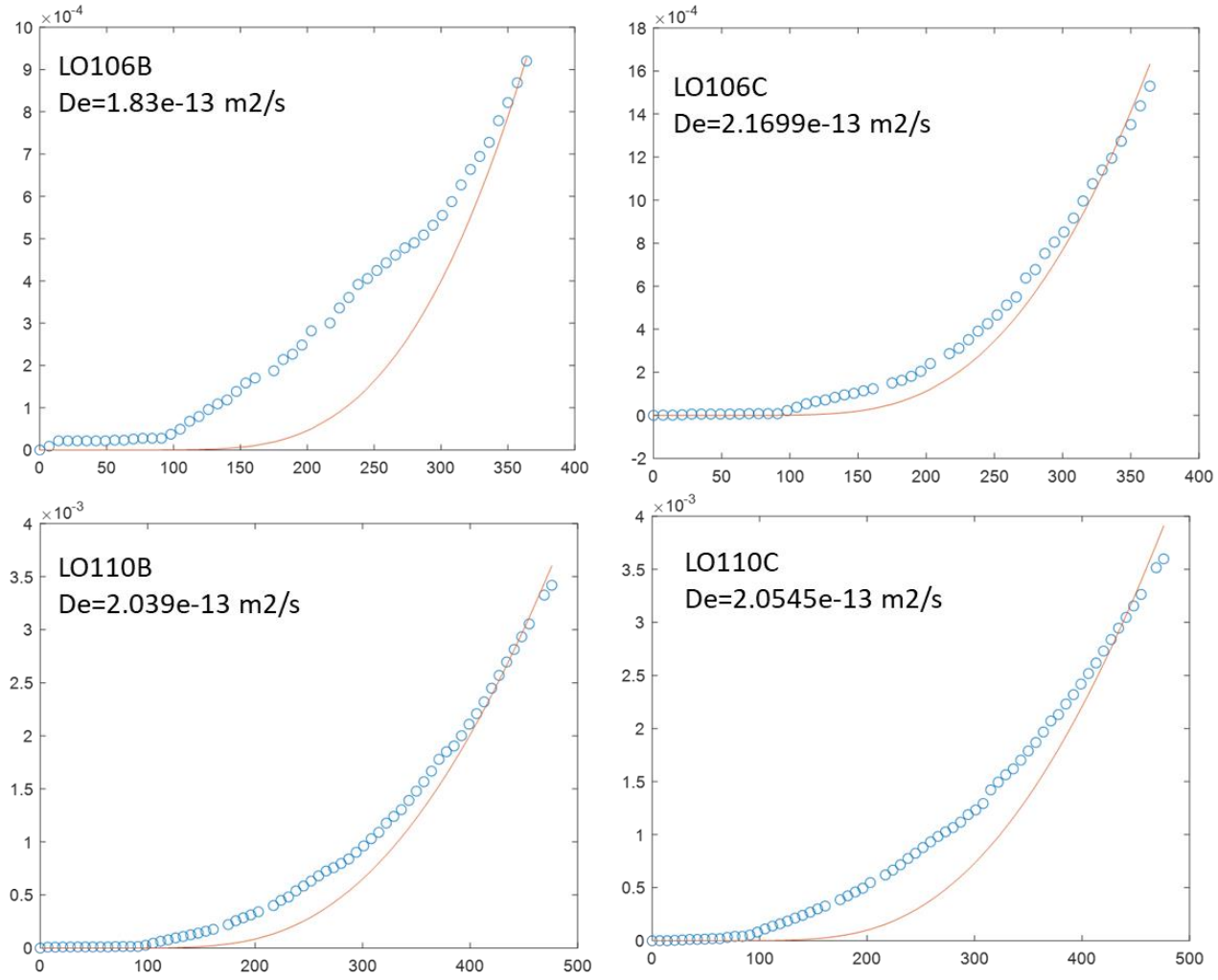

Figure 14 Examples of HTO Through-diffusion modelling. Legend: Blue circles: experimental data; Red line: Modelled fit.

2.4 Conclusion

The year 2024 saw the termination of one set of the parallel through-diffusion experiments of T.1.1 and the subsequent start of the post-mortem autoradiography of T.1.2. The slow diffusion of the tracers continued in 2024, although more data could be gathered and therefore more reliable modelling performed. HTO diffusion appeared to have reached a steady state. Sorbing tracers were however not detected so far in the Outlet chambers. The post-mortem autoradiography performed in T.1.2. showed that the reactive tracers had diffused varying distances into the concrete samples but diffusion fronts had not reached the Outlet chambers. C-14- formic acid had diffused 5 mm in the concrete within 1 year. It had also experienced weak sorption into the cement matrix. Cl-36 had diffused about 8 mm and experienced stronger retention into the cement matrix. Ni-63 post-mortem is still ongoing but results so far indicate negligible diffusion and retention into the cement matrix. In T.1.3, further XCT measurements were performed on the terminated trough-diffusion experiments to obtain structural information to support the result interpretation in other tasks.

The modelling performed in 2024 confirmed the findings in the earlier scoping calculations, that the Loviisa LILW repository basin concrete has rather low diffusivity in the order of 10^{-13} m^2/s, typical for mixed cement-based concretes. The effective diffusion coefficients for HTO were lower than expected based on the scoping calculations, average around $2x10^{-13}$ m^2/s. Modelling for the reactive tracers is still ongoing.

2.5 Plans for year 2025

During year 2025 we will further interpret the results of the though-diffusion experiments started in 2023-2024. The post-mortem autoradiography will be finalised during the year 2025. Samples from different backfill recipes will be studied in 2025. These samples will then be analysed for composition and structure as described in T1.3. Through-diffusion experiments will be started as described in T.1.1., followed by post-mortem autoradiography as in T1.2, if necessary. Diffusion experiment modelling in T.1.4 will continue as experimental results are available.

References

Billon, S., Sardini, P., Leblond, S., Fischet P. 2019. From Bq cm−3 to Bq cm−2 (and conversely)—part 1: a useful conversion for autoradiography. J. Radioanal. Nucl. Chem. 320 (2019), 643-654. https://doi.org/10.1007/s1096 7-019-06521

Delayre, C., Sammaljärvi, J., Billon, S., Muuri, E., Sardini, P. & Siitari-Kauppi, M. Comparison of phosphor screen autoradiography and micro-pattern gas detector based autoradiography for the porosity of altered rocks. Sci. Rep. 10 (2020), 9455. https://doi.org/10.1038/s41598-020-65791-7

Donnard, J., Berny, R., Carduner, H., Leray, P., Morteau, E., Provence, M., NServagent, N., Thers, D. The Micro-Pattern Gas Detector PIM: A Multi-Modality Solution for Novel Investigations in Functional Imaging. Nucl Instrum Methods Phys Res A 610, (2009), 1, 158–160. https://doi.org/10.1016/j.nima.2009.05.186.

Evans, 2008. Binding mechanisms of radionuclides to cement. Cement & Concrete Research, 38 (2008), 543-553.

Isaacs, M., Hinchcliff, J. Felipe-Sotelo, M. & Read, D. 2013. Factors affecting the suitability of superplasticiser-amended cement for the encapsulation of radioactive waste. Advances in Cement Research. Paper 1700099. http://dx.doi.org/10.1680/jadcr.17.00099

Kotatkova, J., Zatloukal, J., Reiterman, P. & Kolar, K. 2017 Concrete and cement composites used for radioactive waste deposition. Journal of Environmental Radioactivity 178-179, 147-155.

Kumpula, Linda; Huhtanen, Iida; Palander, Salla; Ylä-Mella, Mia; Kuhmonen, Venla. 2022. Käytetyn ydinpolttoaineen ja radioaktiivisen jätteen huolto Suomessa: Toinen Euroopan unionin neuvoston direktiivin 2011/70/EURATOM 12 artiklan mukainen kansallinen ohjelma. Työ- ja elinkeinoministeriön julkaisuja 2022:18. ISBN:978-952-327-823-3

L'Annunziata (ed). 2003. Handbook of Radioactivity Analysis. 2nd edition. Pages 1063-1127. ISBN: 9780080495057

Lalan, P., Dauzères, A., De Windt, L., **Sammaljärvi**, J., Bartier, D., Techer, I. Detilleux, V., & Siitari-Kauppi, M. 2019. Mineralogical and microstructural evolution of Portland cement paste/ argillite interfaces at 70 °C – Considerations for diffusion and porosity properties. 2019. Cement and Concrete Research. 115 (2019), 414-425. https://doi.org/10.1016/j.cemconres.2018.09.018

Lefeuvre, H., Donnard, J., Descostes, M., Billon, S., Duval, S., Oger, T., Toubon, H. and Sardini, P. 2022. Spectroscopic autoradiography of alpha particles using a parallel ionization multiplier gaseous detector. Nuclear Instruments and Methods in Physics Research Section A: Accelerators, Spectrometers, Detectors and Associated Equipment, 1035 (2022), 166807. https://doi.org/10.1016/j.nima.2022.166807

Macé, N., Fichet, P., Savoye, S., Radwan, J., Lim, C., Lefèvre, S., Page, J and Henocq, P. 2019. Use of quantitative digital autoradiography techqniue to investigate the chlorine-36-labelled radiotracer transport in concrete. Applied Geochemistry, 100, 326-334.

Mazurier A., Sardini P., Rossi A.M., Graham R.C., Hellmuth K.-H., Parneix J.-C., **Siitari-Kauppi** M., Voutilainen M., Caner L. 2016. Development of a fracture network in crystalline rocks during weathering: Study of Bishop Creek chronosequence using X-ray computed tomography and C-14-PMMA impregnation method. The Geological Society of America Bulletin, 128, 1423-1438.

Möri, A., et al, 2003. The Nagra-JNC in situ study of safety relevant radionuclide retardation in fractured crystalline rock. IV: the in situ study of matrix porosity in the vicinity of a water conducting fracture. Technical Report. 00–08. Nagra, Wettingen/ Switzerland

Neji, M., Dauzères, A., Grellier, A., **Sammaljärvi**, J., Tikkanen, O. and **Siitari-Kauppi**, M. 2022. Comparison of the chemo-mechanical behavior of low-pH cement exposed to calcareous water and to argillite pore water. Applied Geochemistry. 144(2022), 105392. https://doi.org/10.1016/j.apgeochem.2022.105392

Niu, H., Helser, J., Corfe, IJ., **Kuva,** J., Butcher, AR., Cappuyns, V., Kinnunen, P., Illikainen, M., 2022. Incorporation of bioleached sulfidic mine tailings in one-part alkali-activated blast furnace slag mortar, Construction and Building Materials 333, doi: 10.1016/j.conbuildmat.2022.127195

Nummi, O. 2018. Safety Case for Loviisa LILW Repository 2018 - Main Report. LO1-T3552-00023, version 1.1. Fortum Power and Heat Oy.

Sammaljärvi J.,, Shroff Rama, M., Ikonen, J., Muuri, E., Hellmuth, K.-H., Siitari-Kauppi, M. Free radical polymerisation of methacrylates with thermal initiator in clay rock. Eng. Geol. 210 (2016), 70-83. https://doi.org/10.1016/j.enggeo.2016.06.003

Sammaljärvi, J. 2017. Structural characterisation via C-14-PMMA impregnation technique: method and application development. Academic dissertation. Report Series in Radiochemistry, 37/2017.

Sammaljärvi, J.,Xiadong, L., Gaboreau, S., Betelu, S., Donnard, J., Sardini, P., Siitari-Kauppi, M. & Henocq, P. 2024. Autoradiographic imaging of the spatial distribution of Cl-36 in two mortars. Manuscript in Preparation.

Sardini, P., Caner, L., Mossler, P., Mazurier, A., Hellmuth, K.-H., Graham, R., Rossi, A., and Siitari-Kauppi, M. Calibration of digital autoradiograph technique for quantifying rock porosity using 14CPMMA method, J. Radioanal. Nucl. Chem. 303(2014), 1, 2015, 11-23. https://doi.org/10.1007/s10967-014-3617-9

Sardini, P., Angileri, A., Descostes, M., Duval, S., Oger, T., Patrier, P., Rividi, N., **Siitari-Kauppi**, M., Toubon, H. & Donnard, J. 2016. Quantitative autoradiography of alpha particle emission in geo-materials using the Beaver™ system. Nuclear Instruments and Methods in Physics Research Section A: Accelerators, Spectrometers, Detectors and Associated Equipment, 833 (2016), 15-22. https://doi.org/10.1016/j.nima.2016.07.003

Siitari-Kauppi M. 2002. Development of C-14-polymethylmethacrylate method for the characterisation of low porous media – Application to rocks in geological barriers of nuclear waste storage. Academic Dissertation. Report Series in Radiochemistry, 17/2002.

Seigneur, N., L'Hôpital, E., Dauzères, A., **Sammaljärvi**, J., Voutilainen, M., Labeau, P.E., Dubus, A., Detilleux, V. 2017. Transport properties evolution of cement model system under degradation - Incorporation of a pore-scale approach into reactive transport modelling. Physics and Chemistry of the Earth. 99 (2017), 95-109. http://dx.doi.org/10.1016/j.pce.2017.05.007

Solismaa, S., Torppa, A., **Kuva**, J., Heikkilä, P., Hyvönen, S., Juntunen, P., Benzaazoua, M., Kauppila, T., 2021. Substitution of Cement with Granulated Blast Furnace Slag in Cemented Paste Backfill: Evaluation of Technical and Chemical Properties. Minerals, 11, 1068, 18 p. doi: 10.3390/min11101068

Van Es, E., Hinchliff, J., Felipe-Sotelo, M., Milodowski, A.E., Field, L.P., Evans, N.D.M., Read, D. 2015. Retention of chlorine-36 by a cementitious backfill. Mineralogical Magazine, 79(6), 1297-1305.

Wieland, E., Jakob, A., Tits, J., Lothenbach, B., and Kunz, D. Sorption and diffusion studies with low molecular weight organic compounds in cementitious systems. Applied Geochemistry, 67 (2016), 101-117. https://doi.org/10.1016/j.apgeochem.2016.01.009

Young, A.J. 2012. The Stability of Cement Superplasticiser and its Effect on Radionuclide Behaviour. Doctoral Dissertation, Loughborough University, United Kingdom.